Article

Early Stages of Biomineral Formation—A Solid-State NMR Investigation of the Mandibles of Minipigs

Anastasia Vyalikh [1,2,*], **Cindy Elschner** [2], **Matthias C. Schulz** [3], **Ronald Mai** [3,4]
and Ulrich Scheler [2,*] iD

[1] Institute of Experimental Physics, Technische Universität Bergakademie Freiberg,
D-09599 Freiberg, Germany

[2] Leibniz-Institut für Polymerforschung Dresden, e.V., D-01069 Dresden, Germany; elschner@ipfdd.de

[3] Department of Oral and Maxillofacial Surgery, University Hospital "Carl Gustav Carus",
Technische Universität Dresden, D-01307 Dresden, Germany;
Matthias.Schulz@uniklinikum-dresden.de (M.C.S.); ronald.mai@gmx.de (R.M.)

[4] Mund-Kiefer- und Gesichtschirurgie Dr. Dr. Ronald Mai, SN D-01561 Großenhain, Germany

[*] Correspondence: anastasia.vyalikh@physik.tu-freiberg.de (A.V.); scheler@ipfdd.de (U.S.);
Tel.: +49-373-1393-341 (A.V.); Tel.: +49-351-4658-275 (U.S.)

Abstract: Solid-state nuclear magnetic resonance (NMR) spectroscopy allows for the identification of inorganic species during the biomineral formation, when crystallite particles visible in direct imaging techniques have not yet been formed. The bone blocks surrounding dental implants in minipigs were dissected after the healing periods of two, four, and eight weeks, and newly formed tissues formed around the implants were investigated ex vivo. Two-dimensional ^{31}P-^{1}H heteronuclear correlation (HETCOR) spectroscopy is based on the distance-dependent heteronuclear dipolar coupling between phosphate- and hydrogen-containing species and provides sufficient spectral resolution for the identification of different phosphate minerals. The nature of inorganic species present at different mineralization stages has been determined based on the ^{31}P chemical shift information. After a healing time of two weeks, pre-stages of mineralization with a rather unstructured distribution of structural motives were found. After four weeks, different structures, which can be described as nanocrystals exhibiting a high surface-to-volume ratio were detected. They grew and, after eight weeks, showed chemical structures similar to those of matured bone. In addition to hydroxyapatite, amorphous calcium phosphate, and octacalcium phosphate, observed in a reference sample of mature bone, signatures of ß-tricalcium phosphate and brushite-like structures were determined at the earlier stages of bone healing.

Keywords: solid-state NMR; heteronuclear correlation spectroscopy; biomineralization; pre-mineralization stage

1. Introduction

As the main component of vertebrates' hard tissues in bones and teeth, calcium phosphate is the most common biomineral. Unravelling the process of calcium phosphate formation in the biological environment during bone healing or remodeling is a prerequisite for an understanding of the mechanisms of biomineralization and pathological mineralization. This knowledge might lead to novel bioinspired strategies for developing advanced materials as well as preventing and treatment of calcified tissue diseases.

The mechanisms of biomineralization and pathological mineralization still remain a subject of debate. The classical physico-chemical view on nucleation and crystallization based on the association of ions from a supersaturated solution has been revised. In mineralized tissues, a key factor for the

control of the nucleation, growth, and organization of hierarchical structures at different length scales is the presence of the organic matrix, which can either localize crystallization or stabilize the otherwise metastable or unstable amorphous phases [1]. It has been demonstrated that calcium-based biominerals can be formed through a complex multistage process that involves stable pre-nucleation clusters with aggregation and densification into an amorphous precursor phase and subsequent transition into a crystal [2,3]. This formation mechanism for biomineralization has been supported by in vitro studies using a combination of cryo-transmission electron microscopy and molecular modeling [4,5]. Dey et al. demonstrated heterogeneous surface-induced crystallization of hydroxyapatite (HAp) in the presence of a nucleating surface using a model system of simulated body fluid as a mineral source [5]. In the model system, the crystals were never observed together with aggregates of clusters. The in vitro mineralization studies are in agreement with in vivo experiments that have also suggested the involvement of an initial amorphous calcium phosphate phase (ACP) followed by transformation to the final HAp in forming fin bone of zebra fish [6] and in tooth enamel [7]. The degree and the time sequence of mineralization have been studied in human [8] and animal [9] bone tissues. It has been reported that the formation of new bone is a multistep process, within which the new matrix begins to mineralize after about 5–10 days from the time of deposition. The process is followed by increases in the crystal size and the number of crystals, as well as remodeling, and then stops after a period of 30 months, having reached the physiological limit of the mineral content at the tissue level. However, for a detailed understanding of the biomineralization processes, characterization on the molecular scale at all stages, including initial, intermediate, and mature mineralization phases, is required. It has been postulated long ago that ACP is formed from nanometer-sized clusters—so-called Posner's CaP clusters—with a chemical composition $Ca_9(PO_4)_6$, which are the basic units of the final apatite crystals [10]. The identification of the initial mineral phase proved to be a challenging task due to its poor crystallinity, its highly substituted nature, and a very small size of mineral clusters for visualization by microscopy techniques. In contrast to the systems studied in vitro, in organisms, other transient calcium phosphate phases such as brushite (DCPD) and octacalcium phosphate (OCP) have been implicated as phases that are intermediate to the formation of hydroxyapatite (HAp). Indeed, evidence for brushite and OCP has been reported in bone using Raman spectroscopy [11]. This demonstrates that in vivo bone formation may show different behavior compared to biomimic and in vitro grown model systems. Therefore, a detailed study on a molecular level on how biominerals are formed in organisms can shed light on the natural mineralization mechanisms. However, implementation of in vivo experiments tracing various stages of mineralization is difficult to achieve, because any non-destructive method based on real-space imaging such as magnetic resonance imaging (MRI) and computed tomography (CT) will only find structures exceeding a minimal size in space due to their inherent detection limits caused by the limits of the spatial resolution of the particular method.

Solid-state nuclear magnetic resonance (NMR) spectroscopy is ideally suited for the characterization of disordered or nanoscale materials and has been shown to provide important structural information in natural dentine [12,13], cartilage [14], and bone minerals [15–18] and their model compounds [19–23]. The presence of certain moieties known to exist in calcified tissues such as calcium phosphates, hydroxide groups, and water molecules as well as their arrangement and order, can be examined using ^{31}P and ^{1}H solid-state NMR. Two-dimensional ^{1}H-^{31}P heteronuclear correlation (HETCOR) spectroscopy utilizes the distance-dependent heteronuclear dipolar coupling and thus emphasizes spatial proximity between phosphate- and hydrogen-containing species. Therefore it allows for the determination of the nature of inorganic species present at different mineralization stages based on the ^{31}P chemical shift information.

In the present study, we present a molecular-level ex vivo NMR characterization of in vivo grown tissues. Therefore, screw-type dental implants were inserted into the mandibles of minipigs. For ex vivo analysis by solid-state NMR, the bone blocks surrounding the dental implants were dissected after healing periods of two, four, and eight weeks in order to study how biominerals

develop in organisms. The NMR spectra of newly formed tissues were compared to mature bone obtained from the same organism.

2. Results

Figure 1 shows a magnetic resonance (MR) proton density slice image of the bone block of a $20 \times 10 \times 10$ mm^3 size extracted after the healing period of two weeks. The dental implant inserted into the mandibular block and dense mineralized tissue appears dark due to the lack of signal. The adjacent connective tissue is depicted in different gray scales. The red rectangle in Figure 1 indicates the area in a cavity beneath the implant apex, where tissue has grown after the healing period without direct contact to the implant. The proton density and the tissue structure in this region deviate from the surrounding tissues and thus reveal the formation of a new tissue. The morphology and quality of the newly formed tissue has been studied by MRI in the same time steps and published elsewhere [24]. Using solid-state NMR, the composition of newly formed tissue and its promotion with increasing healing time has been investigated in this work.
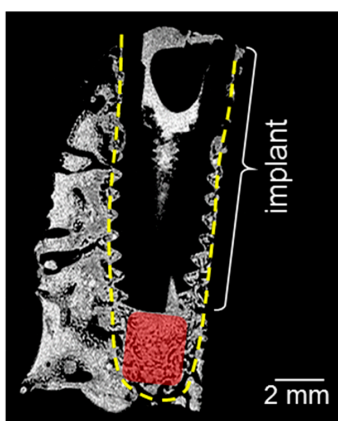

Figure 1. Magnetic resonance (MR) proton density slice image of the bone block containing the implant after a healing time of two weeks. The yellow dotted lines indicate the implant cavity, and the red rectangle shows the region with newly formed tissues, extracted for NMR measurements. The highest proton density is indicated by light gray, the lowest one by black.

Figure 2 shows the ^{31}P magic angle spinning (MAS) NMR spectra of a series of the samples after two, four, and eight weeks of healing, measured by direct polarization (DP) (Figure 2a) and cross-polarization (CP) from ^{1}H (Figure 2b). All ^{31}P MAS NMR spectra from newly formed tissues are very similar irrespective of the healing time, and reproduce the spectrum of the mature bone presented for comparison in Figure 2c (bottom). The DP spectra are characterized by a single, featureless, and almost symmetric line centered at 3.0 ppm with a rather large linewidth of 3.5 ppm. In the literature, the peak at 3 ppm is attributed to ACP, which is known to compose the bone mineral structure [25,26]. The reference spectrum of crystalline HAp shown in Figure 2c is significantly narrower and demonstrates an intrinsic peak at 2.7 ppm.

For selectivity, CP experiments in which signals of the sites in the vicinity of protons were enhanced were subsequently performed. The ^{31}P{^{1}H} CP MAS NMR spectra based on the magnetization transfer from ^{1}H to ^{31}P sites strongly indicated that the ^{31}P species strongly coupled to protons. The CP MAS NMR spectra of newly formed tissues (Figure 2b) demonstrated similar featureless signals centered at ca. 3 ppm. They were characterized by even larger linewidths when compared to the DP spectra. Inhomogeneous broadening of the latter resulted from the distribution in the local environment of ^{31}P sites in close proximity to ^{1}H. The CP spectrum of the 2w sample demonstrated a much weaker intensity compared to other CP spectra, as shown in Figure S3. This is explained by a very low concentration of the phosphorous-containing species due to a nearly complete

absence of mineralized tissue. This is supported by the fact that the newly formed tissue after two weeks appeared as soft rather than hard tissue.
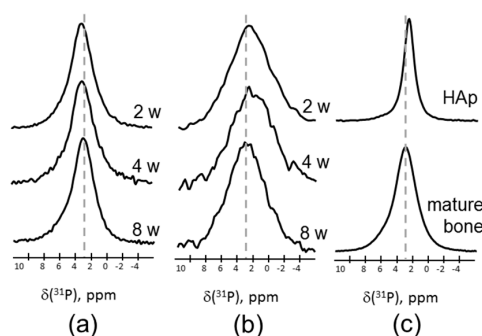

Figure 2. ^{31}P magic angle spinning nuclear magnetic resonance (MAS NMR) spectra of newly formed tissues after two, four, and eight weeks healing time, measured by (**a**) direct polarization (DP), and (**b**) using cross-polarization (CP) from ^{1}H at a contact time of 0.1 ms. (**c**) The ^{31}P MAS NMR spectra of the mature bone (bottom) and hydroxyapatite (top). The spectra are normalized to maximal intensity.

Two-dimensional ^{1}H-^{31}P heteronuclear correlation (HETCOR) spectra of tissues formed after different healing periods as well as the spectrum of mature mandibular bone of a minipig are shown in Figure 3. For assignment, we summarized the data on ^{31}P and ^{1}H chemical shifts previously reported in the literature for various calcium phosphate minerals suggested to be present in bone mineral tissues. This data is shown in Table 1. In the spectrum of bone, two characteristic correlation signals at ca. 0 ppm and 5 ppm in the ^{1}H dimension are assigned, respectively, to PO_4^{3-}/OH^- groups in the apatite structure and to structural/surface water protons spatially related to the mineral phase, according to Yesinowski and Eckert [27]. Similar correlation signals have been observed in synthetic biomimetic nanocomposites [22,28] as well as in biominerals such as animal bone [17,29], joint mineralized cartilage [14], and rat dentine [12].
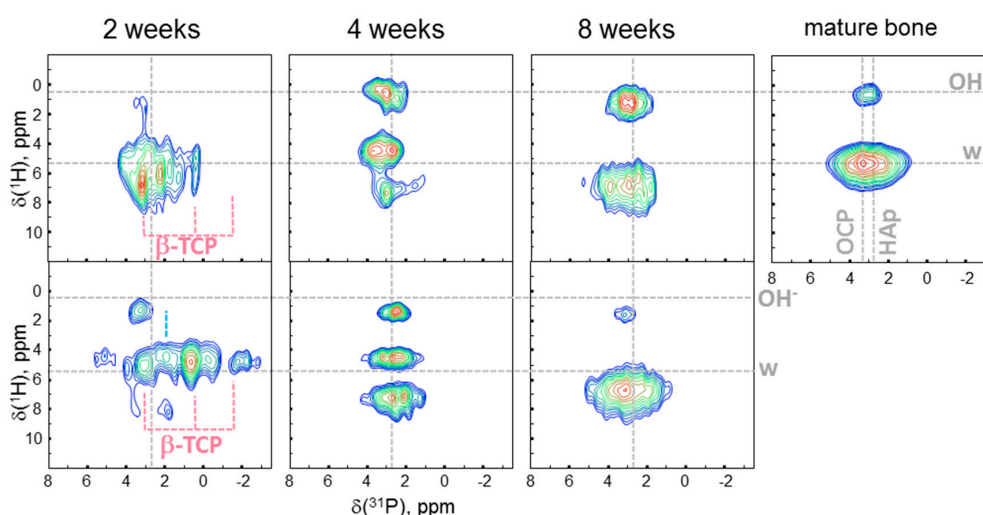

Figure 3. ^{1}H-^{31}P heteronuclear correlation (HETCOR) spectra of the newly formed tissues after two, four, and eight weeks of healing time and of mature bone. For each healing period samples from two animals (top and bottom) were measured. Guidelines at the ^{1}H chemical shifts of 0.2 ppm and 5.4 ppm characteristic of apatitic hydroxides and water, respectively, are shown. In the ^{31}P direction, the guideline at 2.7 ppm characteristic of hydroxyapatite is indicated in all samples. In addition, in the spectrum of mature bone, the guideline at 3.3 ppm, characteristic of octacalcium phosphate (OCP), is shown.

Table 1. [31]P and ^{1}H chemical shift parameters for calcium phosphate structures reported in the literature.

Mineral	Chemical Shift		References
	[31]P, ppm	[1]H, $\pm$0.05 ppm	
HAp, hydroxyapatite	2.8 ± 0.2	0.2 5.5	[25,30,31]
Bru, brushite (dicalcium phosphate, dehydrate)	1.7 ± 0.3	4.1 6.4 10.4	[25,30–33]
Monetite (dicalcium phosphate, anhydrous)	0.0 ± 0.4 −1.5 ± 0.4		[25,30,31,33]
ACP, amorphous calcium phosphate	3.0	5.5	[25,26]
OCP, octacalcium phosphate	−0.2 ± 0.4 1.9	0.18 5.5	[30,31,34]
	3.3 ± 0.3 3.7	13.6	
β-TCP, tricalcium phosphate	−1.6 0.2 2.9		[31,35]

Based on the correlation signals in the ^{31}P dimension, the dominating contribution at 3.3 ppm in mature bone is attributed to octacalcium phosphate (OCP). The presence of HAp at 2.7 ppm and ACP at 3.0 ppm has also been found. The spectra of newly formed tissues show distinct differences to that of mature bone, particularly, at the earlier stages. The two-week (2w) spectra from two different animals represent a complex superposition of low intensity signals, whose maxima are spread from 4 to −2 ppm. After four weeks, the lines become narrower in the ^{31}P direction and split into three distinct contributions in the ^{1}H direction. After eight weeks, the spectra of both samples become more similar to the spectrum of the reference bone yielding only two correlation peaks, well separated in the ^{1}H dimension. The mineral components identified in the 2D spectra at different healing stages and in the mature bone in our work are summarized in Table 2 and discussed in the section below. In the work of Wu et al. [36], the presence of phosphorylated proteins at the very early stages of bone mineralization in chick embryos aged 8–14 days was shown using solid-state NMR. However, by Day 19 of embryonic development, no phosphoproteins could be detected because their signals were overwhelmed by large amounts of inorganic mineral phases. In our study, we performed the ^{31}P slow MAS NMR measurements at −20 °C (see Figure S4), as the phospholipids were expected to show lower shift anisotropy and specific chemical shifts. These additional measurements did not reveal phospholipid signals.

Table 2. The presence of calcium phosphate minerals in the samples under study at different healing stages (ACP = amorphous calcium phosphate; OCP = octacalcium phosphate; Bru = brushite; TCP = tricalcium phosphate; Hap = hydroxiapaptite).

Sample	Mineral Components				
	ACP	OCP	Bru	β-TCP	HAp
2 w	x x	x x	x x	 x	
4 w	x x	x x	x x	 	x x
8 w	x x	x x	 x	 	x x
Mature bone (reference)	x	x			x

3. Discussion

Our results show that solid mineral phosphate species were present in the defect zone around the dental implant in the mandibular bone of minipigs two weeks after implant insertion, although hard tissue had not yet been formed at this stage. The quantitative information available from the DP NMR spectra allowed us to estimate the fractions of mineral and organic components in the tissues after different healing times and to compare it to mature bone. Therefore, we integrated ^{1}H and ^{31}P MAS NMR spectra and calculated the ratio of hydrogen and phosphorous atoms. A spectrum of hydroxyapatite was used for calibration of the respective signal ratios from proton and phosphorous spectra. The contribution from water in the ^{1}H spectra identified by the chemical shift was ignored. The results show a 10-fold increase in the ratio of phosphorous atoms to hydrogen atoms in the organic phase in the four-week (4w) and eight-week (8w) samples when compared to the 2w sample. Moreover, the mineral/organic component ratio remained unchanged after four weeks of healing and was similar to that of the mature bone. This observation is in agreement with the work of Bala et al., who reported that the majority of newly formed tissue within two weeks must be organic soft tissue [9].

In order to follow changes in the mineral phase upon new tissue formation and maturation, 2D HETCOR spectroscopy, which provides spatial correlations between ^{1}H spins (from organic component and water) and ^{31}P spins (primarily phosphate species in the mineral component), was applied. The signal separation available in the 2D spectra provided a higher resolution in the ^{31}P dimension as compared to the 1D ^{31}P spectra and thus allowed local mineral structures to be analyzed based on their chemical shifts. To note, the decreased linewidth in the 2D spectra as compared to the 1D CP spectra is related to the longer mixing time in the former, which results in a narrower distribution of the emphasized components.

The HETCOR spectra in Figure 3 demonstrate the development of the newly formed tissue with healing time. All the 2D correlation peaks in our work were centered within the range from −3 ppm to ca. 5 ppm, corresponding to phosphate groups in various calcium phosphate minerals. The HETCOR spectra of both 2w samples were slightly different. This can be explained by the variation in the concentration and location of the surrounding calcium atoms, because the ^{31}P chemical shift of a phosphate unit is very sensitive to calcium content [37]. Moreover, protonation of the phosphate is also known to lead to an upfield ^{31}P shift [30]. Nevertheless, signatures of ACP, OCP, and brushite (Bru) were found in both 2w samples, and the presence of β-TCP was revealed in only one of them. Such differences might be associated with in vivo interindividual variability and might be explained by the way different animals respond to implant insertion in various ways. Whereas ACP and OCP are known to constitute biological minerals, brushite has been only proposed as an intermediate in biomineralization processes such as bone formation [38] and the dissolution of enamel in acids (dental caries) [39–41]. Hence, we term it here as a brushite-like component. It is worth noting that, although it is a major component of most vertebrate hard tissues, HAp was not found in either 2w sample. Thus, we can conclude that, rather than the formation of biominerals, the pre-stages of biomineralization were observed here. After four weeks, the presence of ACP, OCP, the brushite-like component, and HAp was found in both 4w samples. Finally, at the last stage of healing, ACP, HAp, and OCP were visible in the 8w spectra. This composition is close to that of the mature bone serving as reference, except for the presence of Bru phase in one of two 8w samples. However, this phase could be stabilized by an environment before conversion to hydroxyapatite. To sum up, the general trend in the formation of biomineral tissue with time evolution is clearly observed.

The ^{1}H signals from newly formed tissues strongly deviated from those of mature bone, where the protons related to apatitic OH$^-$ groups and water molecules were found. An absence or undetectable amount of apatitic OH$^-$ groups expected at ca. 0 ppm was observed at all early stages in all samples, except for one 4w sample. This supports reports of a strong deficiency of hydroxide groups in mature bone and dental tissues [12,42,43]. In our previous studies on water absorbance on silica surfaces [44] and on hydroxyapatite-gelatin nanocomposites [22,28], we demonstrated the variation in the ^{1}H chemical shift depending on (1) the dimensionality of the water structures formed on the surface

and related to the strength of hydrogen bonds, and (2) the chemical groups donating hydrogen atoms for hydrogen bond formation. As a fast exchange of hydrogen bonded protons is known to occur at ambient temperatures, the exchanging protons appear in the ^{1}H spectrum at the chemical shift, which is the weighted average of the chemical shifts from the individual structures. Thus, the ^{1}H values discussed here can result from OH groups participating in hydrogen bonding between hydrogenated phosphates, bulk water, isolated water molecules, and organic molecules present in bone (e.g., collagen and non-collagen proteins), giving rise to variability in the ^{1}H shifts of natural bone tissues. Actually, three ^{1}H signals, similar to the 4w samples, have been observed in the biomimetic mesocrystal system of fluoroapatite and the organic matrix at the early growth stage [28]. In the latter, the signals have been attributed to three different water states associated with (i) isolated water molecules, being structural defects in the crystalline mineral domains, (ii) bound water on the mineral surface, and (iii) mobile water included in the amorphous organic layer, where it strongly interacts with organic molecules and inorganic species. The change to two ^{1}H signals in the 8w samples can be associated with the re-organization of complexes between water and protein molecules always present in the organic matrix, and/or crystallite growth, which results in diminishing the contribution from surface bound water due to reduction in the specific surface area. This scenario corroborates the recent biomineralization mechanism that manifests clustering and densification into an amorphous precursor phase [2,3,5]. Our results demonstrate that different calcium phosphate minerals are present in the newly formed tissues at various healing stages, and that hydroxyapatite has not been formed in the tissue after two weeks. This observation supports the next stage in the recent biomineralization mechanism, which involves the final crystallization to hydroxyapatite and agrees well with other studies suggesting a duration of primary mineralization of up to 3 months [8,9].

4. Materials and Methods

4.1. Sample Preparation

Six titanium coated polyetheretherketone (PEEK) implants of a special design—to create a defined area between the implant surface and the round drill hole reported in [24,45]—were inserted in the mandibular bone of minipigs. The mandibles were resected after healing periods of two, four, and eight weeks. The details of the animal model are given in Supplementary Materials. The specimens were stored in a phosphate buffer solution containing penicillin, streptomycin, gentamycin, and amphotericin B at 8 °C. Due to tight fixing of the dental screws, contact of the tissues investigated and phosphate solution was avoided. For the solid-state NMR measurements, species of newly formed tissues were isolated from the host bone, placed into MAS zirconia rotors with an o.d. of 4 mm, tightly capped, and immediately measured. Thus, two samples from different animals were examined after each healing period. The bone serving as reference was obtained from mature pristine mandibular bone and ground in a freezer mill. The reference sample of hydroxyapatite was purchased from Merck KGaA (Darmstadt, Germany) and used without purification. Control measurements of both untreated bone blocks and ground bone after extraction and after storage for 4 weeks—a period during which some samples had to be stored before the solid-state NMR following the MRI experiments—were performed to verify that the storage conditions and grinding did not affect the mineral structure. The results of the control experiments are presented in Figures S1 and S2.

4.2. NMR Imaging Measurements

The NMR Imaging was performed on a 7 T Bruker Avance 300 nonclinical NMR spectrometer (Bruker BioSpin, Rheinstetten, Germany) using a linear polarized rf coil of a 15 mm inner diameter and a BrukerBioSpin Micro 2.5 gradient system generating a maximum magnetic field gradient strength of up to 1 T/m on three axes. For the experiment, the whole bone block was immersed into an NMR tube filled with a perfluorinated fluid (Fluorinert FC 77®, 3M Belgium NV/SA, Zwijndrecht,

Belgium) preventing dehydration and providing a signal-free background. For a proton-density image, a spin-echo multi-slice sequence with a repetition time of 2.5 s, an echo time of 4 ms, a matrix size of 512 × 256 pixel, a slice thickness of 125 μm, and 32 scans was used.

4.3. Solid State NMR

All NMR spectra were obtained on a 7 T Bruker Avance 300 spectrometer operating at resonance frequencies of 300.1 MHz for ^{1}H and 121.5 MHz for [31]P. The ^{31}P NMR experiments were acquired at a spinning frequency of 10 kHz employing a BL4 HXY 4 mm MAS probe head. For ^{31}P MAS NMR spectra, a single 90° pulse with a 3.8 μs pulse duration, a recycle delay of 50 s, a proton decoupling of 50 kHz, and up to 512 repetitions were applied. For [31]P{[1]H} CP measurements, a contact time of 0.1 ms, a ^{1}H decoupling (XiX) of 50 kHz, 4096 repetitions, and a recycle delay of 3 s were used. The spectra were fitted using Dmfit [46]. Two-dimensional [1]H-^{31}P HETCOR experiments were performed using frequency-switched Lee-Goldburg (FSLG) CP with a contact time of 0.5 ms and 1.5 ms and an LG frequency of 75 kHz. A recycle delay of 3 s and 256 scans per t_1 time increment were used. A total of 128 t_1 slices with a 25.2 μs time increment were acquired. Prior to Fourier transform, exponential multiplication with 20 Hz and 30 Hz line broadenings was used in ^{31}P and ^{1}H dimensions, respectively. The ^{1}H chemical shifts were referenced to tetramethylsilane (TMS) at 0 ppm using poly (vinylidene fluoride) as an external reference at 2.9 ppm; powdered ammonium dihydrogen phosphate was used to reference the ^{31}P spectra at 0.72 ppm relative to 85% phosphoric acid.

5. Conclusions

In the present work, the changes in the mineral phase upon new tissue formation and maturation were investigated on the molecular level by applying solid-state NMR. The tissues grown in the cavity beneath the dental implants inserted into the mandibles of minipigs were investigated after three different healing periods of two, four, and eight weeks. While one-dimensional ^{31}P MAS NMR proved the presence of mineralized tissue, two-dimensional heteronuclear correlation HETCOR spectroscopy enabled the detection and identification of various calcium phosphate minerals and water stages during the bone formation. The increase in mineral content was shown by the ratio between the ^{31}P and ^{1}H signal intensities during the healing period. Thus, after two weeks, we observed pre-stages of biomineralization (rather than a formation of biocrystals, which grow in a straightforward manner) with a broad distribution in structural environment. The chemical composition in the newly formed calcium phosphate species varies with healing time until it achieves a composition close to that of mature bone, at approximately eight weeks after healing starts. Besides ACP and OCP phases, revealed in the reference bone spectrum, brushite-like and β-TCP were observed at early stages of mineralization. At the intermediate stage, hydroxyapatite was formed. Our results provide in vivo confirmation of a recently proposed biomineralization mechanism based on the formation of nanometer-sized calcium phosphate clusters, with subsequent aggregation into an amorphous phase and, finally, crystallization to hydroxyapatite. We proved here that solid-state NMR spectroscopy allows for the identification of inorganic species during the biomineral formation at very early stages, when crystallite particles visible in direct imaging techniques have not yet been formed.

Supplementary Materials: The following materials are available online at www.mdpi.com/2312-7481/3/4/39/s1, Figure S1: [1]H-^{31}P heteronuclear correlation (HETCOR) spectra of the bone (a) in block after extraction, (b) cryogenically ground after extraction, (c) in block after storage for 4 weeks in phosphate solution in a fridge and (d) cryogenically ground after storage for 4 weeks in phosphate solution in a fridge. Figure S2: (A) ^{1}H magic angle spinning nuclear magnetic resonance (MAS NMR) spectra, and (B) ^{31}P MAS NMR spectra of the bone in block after extraction, cryogenically ground after extraction, in block after storage for 4 weeks in phosphate solution in a fridge and cryogenically ground after storage for 4 weeks in phosphate solution in a fridge. Figure S3: [31]P{[1]H} CP MAS (10 kHz) spectra of newly formed tissues in the second animal (2w- after two, 4w-four and 8w-eight weeks healing time). The spectra were measured at a contact time of 0.1 ms. Normalization on the sample weight and no line broadening were applied here to demonstrate the sensitivity of the spectra. Figure S4: [31]P{[1]H} CP MAS (2.6 kHz) spectrum of the 2w sample measured at −20 °C.

Author Contributions: U.S. and R.M. conceived and designed the experiments; M.S. performed the preclinical experiments, C.E. contributed to the sample preparation and performed the MRI experiments, A.V. performed the NMR experiments, analyzed the data, and wrote the paper. All authors contributed to the text.

Conflicts of Interest: The authors declare no conflict of interest.

References

1. Wang, L.; Nancollas, G.H. Pathways to biomineralization and biodemineralization of calcium phosphates: The thermodynamic and kinetic controls. *Dalton Trans.* **2009**, 2665–2672. [CrossRef] [PubMed]

2. Gebauer, D.; Völkel, A.; Cölfen, H. Stable prenucleation calcium carbonate clusters. *Science* **2008**, *322*, 1819–1822. [CrossRef] [PubMed]

3. Pouget, E.M.; Bomans, P.H.H.; Goos, J.A.C.M.; Frederik, P.M.; de With, G.; Sommerdijk, N.A.J.M. The initial stages of template-controlled $CaCO_3$ formation revealed by cryo-TEM. *Science* **2009**, *323*, 1455–1458. [CrossRef] [PubMed]

4. Nudelman, F.; Pieterse, K.; George, A.; Bomans, P.H.H.; Friedrich, H.; Brylka, L.J.; Hilbers, P.A.J.; de With, G.; Sommerdijk, N.A.J.M. The role of collagen in bone apatite formation in the presence of hydroxyapatite nucleation inhibitors. *Nat. Mater.* **2010**, *9*, 1004–1009. [CrossRef] [PubMed]

5. Dey, A.; Bomans, P.H.H.; Müller, F.A.; Will, J.; Frederik, P.M.; de With, G.; Sommerdijk, N.A.J.M. The role of prenucleation clusters in surface-induced calcium phosphate crystallization. *Nat. Mater.* **2010**, *9*, 1010–1014. [CrossRef] [PubMed]

6. Mahamid, J.; Sharir, A.; Addadi, L.; Weiner, S. Amorphous calcium phosphate is a major component of the forming fin bones of zebrafish: Indications for an amorphous precursor phase. *Proc. Natl. Acad. Sci. USA* **2008**, *105*, 12748–12753. [CrossRef] [PubMed]

7. Beniash, E.; Metzler, R.A.; Lam, R.S.; Gilbert, P.U. Transient amorphous calcium phosphate in forming enamel. *J. Struct. Biol.* **2009**, *166*, 133–143. [CrossRef] [PubMed]

8. Boivin, G.; Meunier, P.J. The degree of mineralization of bone tissue measured by computerized quantitative contact microradiography. *Calcif. Tissue Int.* **2002**, *70*, 503–511. [CrossRef] [PubMed]

9. Bala, Y.; Farlay, D.; Delmas, P.D.; Meunier, P.J.; Boivin, G. Time sequence of secondary mineralization and microhardness in cortical and cancellous bone from ewes. *Bone* **2010**, *46*, 1204–1212. [CrossRef] [PubMed]

10. Posner, A.S.; Betts, F. Synthetic amorphous calcium phosphate and its relation to bone mineral structure. *Acc. Chem. Res.* **2002**, *8*, 273–281. [CrossRef]

11. Crane, N.J.; Popescu, V.; Morris, M.D.; Steenhuis, P.; Ignelzi, M.A. Raman spectroscopic evidence for octacalcium phosphate and other transient mineral species deposited during intramembranous mineralization. *Bone* **2006**, *39*, 434–442. [CrossRef] [PubMed]

12. Tseng, Y.-H.; Tsai, Y.-L.; Tsai, T.W.T.; Chao, J.C.H.; Lin, C.-P.; Huang, S.-H.; Mou, C.-Y.; Chan, J.C.C. Characterization of the Phosphate Units in Rat Dentin by Solid-State NMR Spectroscopy. *Chem. Mater.* **2007**, *19*, 6088–6094. [CrossRef]

13. Huang, S.-J.; Tsai, Y.-L.; Lee, Y.-L.; Lin, C.-P.; Chan, J.C.C. Structural Model of Rat Dentin Revisited. *Chem. Mater.* **2009**, *21*, 2583–2585. [CrossRef]

14. Duer, M.J.; Friscić, T.; Murray, R.C.; Reid, D.G.; Wise, E.R. The mineral phase of calcified cartilage: Its molecular structure and interface with the organic matrix. *Biophys. J.* **2009**, *96*, 3372–3378. [CrossRef] [PubMed]

15. Cho, G.; Wu, Y.; Ackerman, J.L. Detection of hydroxyl ions in bone mineral by solid-state NMR spectroscopy. *Science* **2003**, *300*, 1123–1127. [CrossRef] [PubMed]

16. Kolodziejski, W. Solid-state NMR studies of bone. *Top. Curr. Chem.* **2005**, *246*, 235–270. [CrossRef] [PubMed]

17. Wilson, E.E.; Awonusi, A.; Morris, M.D.; Kohn, D.H.; Tecklenburg, M.M.J.; Beck, L.W. Three structural roles for water in bone observed by solid-state NMR. *Biophys. J.* **2006**, *90*, 3722–3731. [CrossRef] [PubMed]

18. Jaeger, C.; Groom, N.S.; Bowe, E.A.; Horner, A.; Davies, M.E.; Murray, R.C.; Duer, M.J. Investigation of the Nature of the Protein−Mineral Interface in Bone by Solid-State NMR. *Chem. Mater.* **2005**, *17*, 3059–3061. [CrossRef]

19. Tseng, Y.-H.; Mou, C.-Y.; Chan, J.C.C. Solid-state NMR study of the transformation of octacalcium phosphate to hydroxyapatite: A mechanistic model for central dark line formation. *J. Am. Chem. Soc.* **2006**, *128*, 6909–6918. [CrossRef] [PubMed]

20. Nassif, N.; Martineau, F.; Syzgantseva, O.; Gobeaux, F.; Willinger, M.; Coradin, T.; Cassaignon, S.; Azaïs, T.; Giraud-Guille, M.M. In Vivo Inspired Conditions to Synthesize Biomimetic Hydroxyapatite. *Chem. Mater.* **2010**, *22*, 3653–3663. [CrossRef]

21. Ndao, M.; Ash, J.T.; Stayton, P.S.; Drobny, G.P. The Role of Basic Amino Acids in the Molecular Recognition of Hydroxyapatite by Statherin using Solid State NMR. *Surf. Sci.* **2010**, *604*, L39–L42. [CrossRef] [PubMed]

22. Vyalikh, A.; Simon, P.; Kollmann, T.; Kniep, R.; Scheler, U. Local Environment in Biomimetic Hydroxyapatite−Gelatin Nanocomposites As Probed by NMR Spectroscopy. *J. Phys. Chem. C* **2011**, *115*, 1513–1519. [CrossRef]

23. Vyalikh, A.; Simon, P.; Rosseeva, E.; Buder, J.; Kniep, R.; Scheler, U. Intergrowth and interfacial structure of biomimetic fluorapatite-gelatin nanocomposite: A solid-state NMR study. *J. Phys. Chem. B* **2014**, *118*, 724–730. [CrossRef] [PubMed]

24. Korn, P.; Elschner, C.; Schulz, M.C.; Range, U.; Mai, R.; Scheler, U. MRI and dental implantology: Two which do not exclude each other. *Biomaterials* **2015**, *53*, 634–645. [CrossRef] [PubMed]

25. Aue, W.P.; Roufosse, A.H.; Glimcher, M.J.; Griffin, R.G. Solid-state phosphorus-31 nuclear magnetic resonance studies of synthetic solid phases of calcium phosphate: Potential models of bone mineral. *Biochemistry* **2002**, *23*, 6110–6114. [CrossRef]

26. Combes, C.; Rey, C. Amorphous calcium phosphates: Synthesis, properties and uses in biomaterials. *Acta Biomater.* **2010**, *6*, 3362–3378. [CrossRef] [PubMed]

27. Yesinowski, J.P.; Eckert, H. Hydrogen environments in calcium phosphates: Proton MAS NMR at high spinning speeds. *J. Am. Chem. Soc.* **1987**, *109*, 6274–6282. [CrossRef]

28. Vyalikh, A.; Simon, P.; Rosseeva, E.; Buder, J.; Scheler, U.; Kniep, R. An NMR Study of Biomimetic Fluorapatite—Gelatine Mesocrystals. *Sci. Rep.* **2015**, *5*, 15797. [CrossRef] [PubMed]

29. Santos, R.A.; Wind, R.A.; Bronnimann, C.E. [1]H CRAMPS and [1]H-[31]P HetCor Experiments on Bone, Bone Mineral, and Model Calcium Phosphate Phases. *J. Magn. Reson. Ser. B* **1994**, *105*, 183–187. [CrossRef]

30. Rothwell, W.P.; Waugh, J.S.; Yesinowski, J.P. High-resolution variable-temperature phosphorus-31 NMR of solid calcium phosphates. *J. Am. Chem. Soc.* **1980**, *102*, 2637–2643. [CrossRef]

31. Bak, M.; Thomsen, J.K.; Jakobsen, H.J.; Petersen, S.E.; Petersen, T.E.; Nielsen, N.C. Solid-state ^{13}C and ^{31}P NMR analysis of urinary stones. *J. Urol.* **2000**, *164*, 856–863. [CrossRef]

32. Kaflak-Hachulska, A.; Samoson, A.; Kolodziejski, W. [1]H MAS and [1]H→^{31}P CP/MAS NMR study of human bone mineral. *Calcif. Tissue Int.* **2003**, *73*, 476–486. [CrossRef] [PubMed]

33. Legrand, A.P.; Sfihi, H.; Lequeux, N.; Lemaître, J. ^{31}P Solid-State NMR study of the chemical setting process of a dual-paste injectable brushite cements. *J. Biomed. Mater. Res. B* **2009**, *91*, 46–54. [CrossRef] [PubMed]

34. Davies, E.; Duer, M.J.; Ashbrook, S.E.; Griffin, J.M. Applications of NMR crystallography to problems in biomineralization: Refinement of the crystal structure and ^{31}P solid-state NMR spectral assignment of octacalcium phosphate. *J. Am. Chem. Soc.* **2012**, *134*, 12508–12515. [CrossRef] [PubMed]

35. Obadia, L.; Deniard, P.; Alonso, B.; Rouillon, T.; Jobic, S.; Guicheux, J.; Julien, M.; Massiot, D.; Bujoli, B.; Bouler, J.-M. Effect of Sodium Doping in β-Tricalcium Phosphate on Its Structure and Properties. *Chem. Mater.* **2006**, *18*, 1425–1433. [CrossRef]

36. Wu, Y.; Ackerman, J.L.; Strawich, E.S.; Rey, C.; Kim, H.-M.; Glimcher, M.J. Phosphate ions in bone: Identification of a calcium-organic phosphate complex by ^{31}P solid-state NMR spectroscopy at early stages of mineralization. *Calcif. Tissue Int.* **2003**, *72*, 610–626. [CrossRef] [PubMed]

37. Fletcher, J.P.; Kirkpatrick, R.J.; Howell, D.; Risbud, S.H. [31]P Magic-angle spinning nuclear magnetic resonance spectroscopy of calcium phosphate glasses. *J. Chem. Soc. Faraday Trans.* **1993**, *89*, 3297. [CrossRef]

38. Neuman, W.F.; Bareham, B.J. Evidence for the presence of secondary calcium phosphate in bone and its stabilization by acid production. *Calcif. Tissue Res.* **1975**, *18*, 161–172. [CrossRef] [PubMed]

39. Kodaka, T.; Ohohara, Y.; Debari, K. Scanning electron microscopy and energy-dispersive X-ray microanalysis studies of early dental calculus on resin plates exposed to human oral cavities. *Scanning Microsc.* **1992**, *6*, 475–486. [PubMed]

40. LeGeros, R.Z.; Orly, I.; LeGeros, J.P.; Gomez, C.; Kazimiroff, J.; Tarpley, T.; Kerebel, B. Scanning electron microscopy and electron probe microanalyses of the crystalline components of human and animal dental calculi. *Scanning Microsc.* **1988**, *2*, 345–356. [PubMed]

41. Jin, Y.; Yip, H.-K. Supragingival Calculus: Formation and Control. *Crit. Rev. Oral Biol. Med.* **2002**, *13*, 426–441. [CrossRef] [PubMed]

42. Loong, C.-K.; Rey, C.; Kuhn, L.T.; Combes, C.; Wu, Y.; Chen, S.-H.; Glimcher, M.J. Evidence of hydroxyl-ion deficiency in bone apatites: An inelastic neutron-scattering study. *Bone* **2000**, *26*, 599–602. [CrossRef]

43. Vyalikh, A.; Mai, R.; Scheler, U. OH^- deficiency in dental enamel, crown and root dentine as studied by ^1H CRAMPS. *Bio-Med. Mater. Eng.* **2013**, *23*, 507–512. [CrossRef]

44. Vyalikh, A.; Emmler, T.; Grünberg, B.; Xu, Y.; Shenderovich, I.; Findenegg, G.H.; Limbach, H.-H.; Buntkowsky, G. Hydrogen Bonding of Water Confined in Controlled-Pore Glass 10–75 Studied by ^1H-Solid State NMR. *Z. Phys. Chem.* **2007**, *221*, 155–168. [CrossRef]

45. Stadlinger, B.; Hintze, V.; Bierbaum, S.; Möller, S.; Schulz, M.C.; Mai, R.; Kuhlisch, E.; Heinemann, S.; Scharnweber, D.; Schnabelrauch, M.; et al. Biological functionalization of dental implants with collagen and glycosaminoglycans-A comparative study. *J. Biomed. Mater. Res. B* **2012**, *100*, 331–341. [CrossRef] [PubMed]

46. Massiot, D.; Fayon, F.; Capron, M.; King, I.; Le Calvé, S.; Alonso, B.; Durand, J.-O.; Bujoli, B.; Gan, Z.; Hoatson, G. Modelling one- and two-dimensional solid-state NMR spectra. *Magn. Reson. Chem.* **2002**, *40*, 70–76. [CrossRef]